# Effect of boundary layer low-level jet on fog fast spatial propagation

Shuqi Yan[1], Hongbin Wang[1,*], Xiaohui Liu[2], Fan Zu[1], Duanyang Liu[1,*]

[1]Key Laboratory of Transportation Meteorology of China Meteorological Administration, Nanjing Joint Institute for Atmospheric Sciences, Nanjing, 210041, China
[2]Merchant Marine College, Shanghai Maritime University, Shanghai, 201306, China

*Correspondence to*: Hongbin Wang (kaihren@163.com); Duanyang Liu (liuduanyang2001@126.com)

**Abstract.** The spatiotemporal variation of fog reflects the complex interactions among fog, boundary layer thermodynamics and synoptic systems. Previous studies revealed that fog can present fast spatial propagation feature and attribute it to boundary layer low-level jet (BLLJ), but the effect of BLLJ on fog propagation is not quantitatively understood. Here we analyze a large-scale fog event in Jiangsu, China from 20 to 21 January 2020. Satellite retrievals show that fog propagates from southeast coastal area to northwest inland with the speed of 9.6 m/s, which is three times larger than the ground wind speeds. The ground meteorologies are insufficient to explain the fog fast propagation, which is further investigated by WRF simulations. The fog fast propagation could be attributed to the BLLJ occurring between 50 and 500 m, because the wind speeds (10 m/s) and directions (southeast) of BLLJ core are consistent with fog propagation. Through sensitive experiments and process analysis, three possible mechanisms of BLLJ are revealed: 1) The abundant oceanic moisture is transported inland, increasing the humidity of boundary layer and promoting condensation; 2) The oceanic warm air is transported inland, enhancing the inversion layer and favouring moisture accumulation; 3) The moisture advection probably promotes low stratus formation, and later it subsides to be ground fog by turbulent mixing of fog droplets. The fog propagation speed would decrease notably by 6.4m/s (66%) in the model if the BLLJ-related moisture and warm advections are turned off.

## 1. Introduction

Fog is a kind of low-visibility weather phenomenon that occurs at near surface, causing adverse impacts on traffic transportation. The formation, development and dissipation of fog are the comprehensive results of the interactions among radiation, moisture, microphysics, turbulence, aerosols and other factors (Gultepe et al., 2007; Koračin et al., 2014; Nakanishi, 2000). The relations of fog with meteorological factors are highly variable under different conditions. Therefore, the mechanism of fog evolution needs to be intensively studied.

Under favourable conditions, the fog intensity or its spatial extent can develop extraordinarily fast with time. Field observations conducted at single site reveal that visibility in fog can deteriorate drastically, from about 1km to less than 200m within 30min (Li et al., 2019). It is referred to as fog burst reinforcement, which is firstly raised by Korb et al. (1970) and systematically reviewed by Liu et al. (2012) and Li et al. (2019). Fog burst reinforcement is accompanied by the drastic formation of fog droplets, sudden increase of fog liquid water and broadening of droplet spectrum (Liu et al., 2017; Liu et al., 2021). Additionally, fog can develop rather fast in spatial extent, i.e., the fast spatial propagation of fog (Zhu et al., 2022). It is reflected by the successive visibility dropping in space along a certain direction. The influencing factors of fast spatial propagation could be more complex than that of the burst reinforcement at single site, which have received fewer quantitative studies recently.

Synoptic systems and planetary boundary layer (PBL) thermodynamic structures are key to understanding the cause of fog burst reinforcement and fast propagation. Weak cold air invasion and radiative cooling is an important factor for fog burst reinforcement and fast propagation (Liu et al., 2011; Wang et al., 2020). Dhangar et al. (2021) demonstrated that the radiative cooling at surface and fog top can increase supersaturation and promote fog vertical development. Shen et al. (2022) found that the different cooling rates at two nearby stations lead to a remarkable difference in fog formation time, fog duration and vertical extent. Sufficient water supply is also an important factor. Wobrock et al. (1992) revealed that the role of moisture advection outweighs radiative cooling in large-scale fog events. Pu et al. (2008) found that two layers of moisture advection enhance fog development and maintenance. Under stable synoptic systems, the PBL thermodynamic can also favour fog burst reinforcement and fast fog propagation. The formation of dense fog is usually accompanied by strong inversion layer, of which the intensity could reach 16K/100m (Pu et al., 2008; Liu et al., 2012). Liu et al. (2016) found that upper-level warm advection and low-level cold advection significantly enhance inversion intensity and promote fog development. The vapor advection resulting from southerly winds further increases fog intensity. Appropriate turbulence also facilitates fog formation and enhancement (Ye et al., 2015; Zhou and Ferrier, 2008). Turbulent results in the exchange of heat and moisture within PBL, e.g., the downward entrainment of vapor and cold air can promote condensation and droplet formation (Liu et al., 2016; Zhang et al., 2005). Other studies highlight the role of hygroscopic aerosols and aerosol indirect effects in strong fog events (Boutle et al., 2017; Quan et al., 2021; Shao et al., 2023; Wang et al., 2023; Yan et al., 2021).

Previous studies find that the large-scale fog events are accompanied by boundary layer low-level jet (BLLJ), and try to attribute the spatial propagation of fog to BLLJ. The causes of BLLJ include such as synoptic systems, terrian effect and inertial oscillation (Kraus et al., 1985). Tian et al. (2019) demonstrated that the warm-and-wet southerly BLLJ favours water vapor transportation and inversion layer construction, and later the fog is triggered by a weak cold front invasion. Wu et al. (2020) found that strong northerly BLLJ associated with cold air can destroy inversion layer and lead to early dissipation of fog, while weak BLLJ can promote fog maintenance. Li et al. (2012) revealed that the strengthened turbulence generated by BLLJ wind shear promotes vertical mixing and facilitates fog development. However, the relations between BLLJ and fog propagation and the key synoptic factors have not been quantitatively addressed. Also, the current horizontal and vertical observations are not sufficient to reveal the mechanism of fog propagation. It requires further investigation by numerical models.

In this work, we study a large-scale fog event with fast propagation feature occurring in Jiangsu Province, China from 20 to 21 January 2020. By combination of observations and numerical simulations, we aim to quantitatively reveal the BLLJ effect on fast fog propagation to and identify the key impact factors and mechanisms. This work is expected to better understand the complex interactions among synoptic systems, PBL thermodynamics and fog spatial propagation, as well as provide prediction indicators for operational fog forecast. The study is organized as follows: Section 2 describes the data, methods and numerical models of this study. Sections 3.1 to 3.4 analyze the fog propagation feature and PBL characteristics. Section 3.5 quantitatively study the BLLJ effect on fast fog propagation and identifies key influencing factors. Section 4 concludes the findings of this study.

# 2. Data, methods and model configuration

## 2.1 Data and study area

This study focuses on the Jiangsu area, China (Figure 1), where a large-scale fog event occurred from 20 to 21 January 2020. We collected the data from 70 ground automatic weather stations (AWS) in Jiangsu Province, China. The data is recorded by every 10 minutes, including visibility, temperature, relative humidity (RH), wind direction and wind speed. This data is used to analyze the temporal variation of meteorology, as well as evaluate the model performance on temperature, RH and wind. Additionally, the Sheyang (SY; 120.25 °E, 33.76 °N; 3m) station is a sounding station that used for model evaluation in the vertical direction. The sounding observations include temperature, RH, wind direction and wind speed which are sampled each second. It is conducted twice a day (00UTC and 12UTC).

The geostationary satellite Himawari 8 (https://www.eorc.jaxa.jp/ptree/index.html) is used to retrieve nighttime fog area and evaluate the model performance of fog simulation. The high spatiotemporal resolution (2km in space and 1h in time) is suitable for detecting the fast evolution of fog area. This satellite observation includes 16 bands, and the bands at 3.9 and 11.2 µm are used.

The ERA5 reanalysis data (https://cds.climate.copernicus.eu/cdsapp#!/dataset/reanalysis-era5-pressure-levels) is used to analyze synoptic conditions and provide initial & boundary fields for model simulation. The grid resolution is 0.125 ° (about 12.5km) and the time interval is 6h. All the time in this study is local time (UTC+8).

## 2.2 Methods

### 2.2.1 Satellite fog retrieval

Since the ground AWS stations are not sufficiently fine in spatial resolution, the high spatiotemporal resolution product of Himawari 8 is suitable to study the propagation of fog. Nighttime fog has notable different optical properties at the bands of 3.9µm and 11.2µm, so it can be indicated by the dual-band brightness temperature difference ($Tbb_{3.9}$ minus $Tbb_{11.2}$) lower than a threshold (Cermak et al., 2008). In this study, the threshold is determined to be -2 K following the dynamic threshold algorithm proposed by Di Vittorio et al. (2002). Daytime fog after 08:00 is not retrieved because we mainly focus on the formation and development stage of fog before 08:00.

### 2.2.2 Fog propagation speed calculation

We calculate the propagation speed according to satellite retrieved fog area. At 22:00 on 20 January 2020, a tiny fog area appeared at Nantong and Yanchen coastal region with an area smaller than 50km2 (figure not shown). The center of this fog area is set as point A (120.6 °E, 32.9 °N). We draw a line starting from A with an arbitrary direction, and find its intersection with the fog boundary area at 07:00 next day (point B). Then the propagation speed in this direction can be calculated by the distance from A to B divided by 9 hours (22:00~07:00). By looping from 0 to 360 with the interval of 1°, propagation speeds in all directions are calculated, and the maximum speed is defined as the fog propagation speed.

The fog propagation speed is verified by AWS data. We select three representative stations along the fog propagation direction, Dafeng (DF; 120.48°E, 33.20°N, 14m), Baoying (BY; 119.30°E, 33.23°N, 15m), Sihong (SH; 118.22°E, 33.48°N, 13m) (Figure 1). According to their distances and the time differences when visibility drops to 200m, the propagation speed between two adjacent stations is calculated.

2.2.3 Process analysis on fog

The simulated fog is indicated by fog liquid water content (LWC). Process analysis is used to quantify the contribution of each physical process to LWC variation (Schwenkel et al., 2019; Yan et al., 2020). The variation of LWC is related to the following terms:

$$\frac{\partial \mathrm{LWC}}{\partial t} = \underbrace{-\left(u\frac{\partial}{\partial x}+v\frac{\partial}{\partial \mathrm{y}}+w\frac{\partial}{\partial z}\right)}_{\mathrm{Advc}}\mathrm{LWC} + \left(\frac{\partial \mathrm{LWC}}{\partial t}\right)_{\mathrm{Vmix}} + \left(\frac{\partial \mathrm{LWC}}{\partial t}\right)_{\mathrm{Cond}} + \left(\frac{\partial \mathrm{LWC}}{\partial t}\right)_{\mathrm{Sedi}} + \left(\frac{\partial \mathrm{LWC}}{\partial t}\right)_{\mathrm{other}}$$

where Advc includes horizontal and vertical advection, Vmix is associated with the fog droplet vertical exchange by turbulent mixing, Cond is the vapor condensation (negative means droplets evaporation), Sedi is fog droplets sedimentation. Other microphysical processes include autoconversion, accretion and cold phase processes. They are much smaller than the previous four processes, so they can be safely ignored.

## 2.3 Model configuration and experiments

The Weather Research and Forecasting model (WRF) is implemented to study the fast spatial propagation of fog events. Two domains are set up (Figure 1). The parent domain covers East China, with the grid size of 181×181 and grid interval of 9 km. The nested domain covers Jiangsu Province and its coastal area, with the grid size of 199×199 and grid interval of 3 km. To simulate the turbulent process more reasonably, the vertical levels are refined to 42 levels, with 25 levels under 1500m and 9 levels under 100m (Yang et al., 2019; Yan et al., 2020). The first model level is about 4m. The model is driven by the initial and boundary field from ERA5 Reanalysis. The simulation starts at 08:00 on 19 January and ends at 08:00 on 21 January 2020, with the first 24h as spin-up period. All the time in this study is local time (UTC+8).

Fog is hard to be simulated or predicted well (Zhou et al., 2010, 2012), which is sensitive to the choice of parameterization schemes (Steeneveld et al., 2014; van der Velde et al., 2010). Through massive tests, the QNSE boundary layer scheme (Sukoriansky et al., 2005) and Pleim-Xiu land surface scheme (Pleim et al., 2009) yield the best simulation performance. Other parameterization schemes are listed in Table 1. The simulated fog is indicated by the liquid water content (LWC) greater than 0.015g/kg under the height of 500m, which corresponds to horizontal visibility less than 1km (Kunkel, 1983).

Apart from the base experiment, three sensitive experiments are performed to elucidate the mechanism of fast fog propagation (Table 1). The experiment "Tadv0" turns off the temperature advection within PBL during the fog period. The experiment "QvAdv0" and "QcAdv0" are the same as "Tadv0" except that turning off water vapor advection and cloud water advection, respectively. The experiment "NoAdv" turns off all the advections above. Therefore, the differences of the base experiment with Tadv0, QvAdv0, and Qcadv0 represent the effect of temperature advection, moister advection, and cloud water advection, respectively. The reasons and results of the sensitive experiments will be discussed in Section 3.5.

# 3. Results

## 3.1 Fog overview and synoptic background

The studied fog event occurs at the night of 20 January and dissipates in the daytime of 21 January 2020 (Figure 2). Figure 3 shows the synoptic situations at 08:00 and 20:00 on 20 January. At 500hpa, a frontal zone is located north of 38°N. The Jiangsu area is dominated by prevailing westerly flows with no obvious troughs. At 850hpa, a ridge moves eastward and controls Jiangsu area. The descending motions associated with the ridge and the nocturnal radiative cooling at ground favour the establishment of inversions. At ground level, a weak cold high pressure moves eastward with the central pressure of 1030hpa. The Jiangsu area is dominated by uniform pressure field with small wind speeds, which strengthens atmospheric stratification stability and promotes the accumulation of aerosols and moisture. The moisture condition in Jiangsu is additionally favoured by the water vapor transportation from ocean by easterly winds at 20:00. Under this conductive situation, the fog event occurred from nighttime of 20 to daytime of 21 January over Jiangsu Province (Figure 2).

## 3.2 Fog and ground meteorology variation

Hourly Himawari 8 satellite image clearly shows the spatial propagation of fog (Figure 2). The fog initials at 22:00 on 20 January in Nantong and Yanchen coastal region with an area smaller than $50km^2$. Later, this small fog area expands to a large-scale fog. Specifically, the southeast side of fog area varies relatively slowly, but the northwest side expands remarkably, indicating a large propagation speed. At 07:00 on 21 January, the front of fog expands to Anhui Province. After 07:00, the fog begins to dissipate, and it fully disappears at 11:00 (figure not shown). Figure 4 quantitatively describes the propagation direction and speed of fog. From the east to south directions (the fourth quadrant), fog propagation speed is less than 3m/s. In the west-northwest and west directions, fog propagation speed is larger than 6m/s, and the maximum propagation speed is 9.6m/s occurring at 160° direction (in Cartesian coordinate system). The fast propagation of fog is also reported previously in Jiangsu area (Gao et al., 2023; Zhu et al., 2022), where the fog propagates from coastal area to west boundary of Jiangsu within about 10h.

Visibilities at three representative stations, Dafeng (DF), Baoying (BY) and Sihong (SH) are used to verify the fog propagation speed calculated by satellite (Table 2; Figure 5). At DF, fog forms (visibility less than 1km) early at 19:45 on 20 January. The visibility drops sharply at 23:15 and reaches the minimum at about 00:15. At BY and SH, fog forms in turn, and their visibilities also have burst decreasing feature at 03:40 and 07:00, respectively. We calculate the fog propagation speed by the distances among stations and the time differences when visibility drops to 200m. The propagation speed is 7.6 m/s between DF and BY and 8.3 m/s between BY and SH. These values correspond to the speed calculated by satellite observation.

Figure 5 shows the variation of other meteorological fields. We focus on the characteristics from fog formation to the burst visibility dropping (indicated by yellow dashed lines). At DF, the northerly wind decreases to lower than 1.5m/s at fog formation, which causes the weak cold advection and temperature decreasing. The temperature keeps decreasing and favours the burst reduction of visibility at 23:15. The vapor content (indicated by dew point) increases sharply before 17:00 and decreases slightly since then, so the RH increasing after fog formation is caused by temperature drop. At BY and SH, the wind directions are dominantly southeast and the speeds are generally less than 2m/s before fog formation. The temperature keeps decreasing and vapor content keeps increasing, leading to the further reduction of visibility. Later, the southeasterly winds obviously enhance by about 1m/s, which may contribute to the burst visibility dropping due to the intensified vapor advection from ocean.

The preliminary cause of fog formation and intensification are summarized. As located near the ocean, the moisture at DF reaches the maximum prior to fog formation, so the fog formation and intensification are largely caused by radiative cooling and weak cold advection. At BY and SH, the temperature cooling rate is weaker than DF, which is partly due to the weak warm advection by southeasterly winds. The vapor advection by southeasterly winds favours fog development, and the burst decrease in visibility coincides with the increase in wind speed. Therefore, deduced from BY and SH, the vapor transportation associated with southeasterly winds could be an important reason for northwesterly propagation of fog. However, it is obvious that the ground wind speed is rather small compared with fog propagation speed. Statistics on AWS stations show that although wind direction (east, southeast and south winds at 70% stations) is generally in accordance with fog propagation direction, wind speed is lower than 3m/s at 97% stations from 22:00 to 07:00, which is about one-third of the fog propagation speed. Therefore, the ground meteorological field is insufficient to explain the fast propagation of fog. The fog PBL characteristics and the key influencing factors need to be investigated by numerical simulations.

## 3.3 Model evaluation

Figure 6a evaluates the model performance on temperature, relative humidity (RH) and wind field at surface. The simulated temperature and RH agree well with observations, with the root mean square error (RMSE) of 1.0K and 11%, respectively. The simulation reasonably captures the wind direction transition from north to east, and the RMSE is less than 1m/s.

Figure 6b evaluates the model performance on temperature, RH and wind field in the vertical direction at SY sounding station. The temperature profile is simulated well by the model, with the mean bias of less than 1K. The RH bias is relatively small below about 200m, while it is a bit larger above 200m at 08:00 on 21 January. The simulated wind speed and direction are basically consistent with observation. The large winds (greater than 6m/s) at about 200m are well reproduced by the model, indicating that the model reasonably simulates boundary layer low-level jet. Studies on boundary layer low-level jet are presented in next sections.

Figure 2 compares the satellite observed and simulated fog area. The simulation is only evaluated before 07:00, because the dissipation of fog after 08:00 is not the focus in this study. The model reasonably captures the spatiotemporal evolution of fog, with a slight overestimation of 5~10% in fog area.

Overall, the simulation reasonably captures the temporal variation of meteorology and reproduces the spatial propagation of fog. It establishes the basis for discerning the mechanism of fog propagation.

## 3.4 Characteristics of fog and PBL structure

The thermodynamic variation of PBL is crucial for understanding the propagation of fog. Figure 7a shows the temporal variation of horizontal winds in vertical directions. The simulated wind speed is consistently smaller than 4m/s under about 30m, while it remarkably increases with height. At 18:00 on 20 January, a large wind speed zone (>6m/s) forms at the height between 50 and 500m in the east of 120°E. Since then, the large wind zone moves westward quickly accompanied by wind speed increasing. During the fog period, the average wind speed exceeds 6m/s at the height between 50 to 500m (Figure 7b), which is commonly larger than the wind speed in most fog events. Here, we refer to this large wind speed zone as boundary layer low-level jet (BLLJ). The existence of BLLJ is supported by ERA5 reanalysis on 1000hpa and 975hpa levels (Figure 7b).

The formation of BLLJ is likely caused by the easterly movement of a high pressure at 1000hpa over East China. The central pressure gets enhanced, which strengthens the pressure gradient over Jiangsu area and favours wind speed increasing (figure not shown). The jet core (maximum wind speed) occurs at about 1000hpa (200m), with the time-averaged speed of 10m/s (Figure 7b). At that level, the dominant wind direction is southeast and the wind speed over fog area is 8~16m/s (Figure 7c), which can fit the propagation direction and speed of fog. Also, the expansion speed of vertical fog zone is comparable to the movement speed of jet core (Figure 7a). Therefore, we hypothesize that the southeasterly BLLJ could account for the fast propagation of fog.

Previous studies reveal that southerly BLLJ can transport abundant water vapor to China inland and thus promote fog formation (Liu et al., 2016; Tian et al., 2019). Figure 8 shows the temporal variation of water vapor mixing ratio (Qv) profiles. Since the vapor content over the ocean is higher, it is transported to inland areas by southeasterly BLLJ. The BLLJ can further increases the Qv in PBL by wind speed horizontal convergency and vertical shear. The larger wind speed in BLLJ zone and lower wind speed outside BLLJ zone cause wind speed convergence, which favours the increase in PBL moisture. Additionally, the turbulence generated by vertical shear of wind speed can promote vapor turbulent mixing, leading to the higher Qv above surface being entrained downward and increasing the ground Qv (Gao et al., 2007). The Qv under 300m is generally higher than 3g/kg under the effect of BLLJ. Wu et al. (2020) also found that BLLJ continuously transports water vapor to fog layer, resulting in surface Qv higher than 3g/kg. It is notable that the expansion of vertical fog area coincides with the movement of the zone of Qv>4g/kg. Therefore, moister advection by BLLJ could be an important reason for fast fog propagation.

BLLJ is reported to result in warm advection and deepen inversion layer previously (Tian et al., 2019), and inversion layer is an important reason for fog burst reinforcement in most fog cases (e.g., Li et al., 2019; Liu et al., 2012; Jiao et al., 2016). Figure 9 shows the temporal variation of temperature profile and inversion layer. The inversion layer here refers to the height above ground where temperature monotonically decreases with height. Since 20:00 on 20 January, the ground temperature keeps decreasing due to radiative cooling. Within the fog area, the temperature drop is more significant, which is due to the longwave radiative cooling by fog droplets (Bott, 1991; Jia et al., 2018). Approximately above the fog top, there is an obvious warm air mass transported from ocean to inland areas. The BLLJ-induced warm advection increases vertical temperature gradient and strengthens atmospheric stability. Accordingly, the inversion height over non-fog areas basically keeps increasing. The approximate inversion layer height is about 100~300m, which is consistent with previous studies (Dorman et al., 2021; Li et al., 2019). The maximum inversion intensity of 15K/100m, which is also reported in a dense fog event (16K/100m) by Pu et al. (2008). It favours the accumulation of vapor and condensation nuclei, which is also a possible reason for fog formation in the downstream area.

Additionally seen from Figure 9, the west boundary of vertical fog region below about 100m has a negative slope, i.e., fog forms at upper level ahead of forming at ground. The upper-level fog with no ground contact is referred to as low stratus. The height at which fog/low stratus firstly forms is shown in Figure 10. An initial fog area forms at ground level before 00:00 on 21 January. Since then, low stratus forms at upper level (about 10~66m) over the downstream area, while the ground fog in downstream area forms about 0~20min later than low stratus. The formation of low stratus may also be caused by the BLLJ-induced moisture advection. In addition, the cloud water advection (Section 2.2.3) to downstream area by BLLJ could also be a potential reason. We hypothesize that the formation of ground fog is partly favoured by the stratus lowering, which has been reported by previous studies (e.g., Haeffelin et al., 2010; Liu et al., 2012); the base height of stratus can be smaller than 100m before fog formation (Dupont et al., 2012; Fathalli et al., 2022), which is basically close to our results (10~66m in Figure 10). While in this event, the stratus lowering phenomenon remains to be verified by additional high-spatiotemporal resolution vertical observations.

According to above results, three potential factors for fog propagation are raised: BLLJ-related temperature advection, moisture advection and cloud water advection. These advections possibly promote low stratus formation within 100m above surface, and subsequently the low stratus could subside to be ground fog by the turbulent mixing or sedimentation of cloud droplets. Currently, their contributions to fog propagation have not been quantitatively revealed. Therefore, it will be addressed in the next section.

## 3.5 Quantitative reasons for fast fog propagation

Four sensitive experiments, Tadv0, QvAdv0, QcAdv0 and NoAdv0 (Section 2.3) are conducted to quantify the respective contributions of temperature advection, moister advection, cloud water advection and all these advections to fog propagation (Figure 11). Under the condition with no advections (Figure 11a-d), there is a 80% decrease in fog area and a 6.4m/s (66%) decrease in propagation speed, which highlights the role of BLLJ-related advections. When turning off temperature advection (Tadv0) (Figure 11e-h), the original fog area in the base experiment shrinks 50% in size and breaks into separate fog patches, and the propagation speed decreases by about 5.2m/s (54%). When turning off moisture advection (QvAdv0) (Figure 11i-l)., the fog area shrinks by 62% in size and the propagation speed decreases by about 4.6m/s (48%). When turning off cloud water advection (QcAdv0) (Figure 11m-p), the fog area nearly keeps unchanged during 00:00~04:00 and decreases moderately in size (about 25%) at 06:00 The propagation speed decreases moderately by 2.4m/s (25%). Deduced from the changes in fog area and propagation speed under various experiments, we can infer that the BLLJ-related warm and moisture advection, especially moisture advection, could be the major cause of fast spatial propagation, while cloud water advection has a minor contribution.

We further perform process analysis on LWC (Section 2.2.3) to illustrate the mechanism of fog propagation (Figure 12). The horizontal and vertical values of Advc and Sedi are at least one order of magnitude smaller than that of Cond and Sedi, indicating that cloud water transportation to downstream areas and droplet sedimentation to ground are not the causes of fog propagation. At 00:00 on ground level, Cond is positive over the newly formed fog area (blue and cyan colors surrounding the fog area), indicating that fog firstly forms at ground by radiative cooling before 00:00. After 02:00, Cond is almost negative over the entire fog area, indicating that fog does not firstly form at the ground level (otherwise Cond would have positive values). The formation of ground fog may be contributed by the LWC turbulent entrainment from upper level, because Vmix shows significant positive values after 02:00. In the vertical direction, Vmix and Cond are still two dominant physical processes (Figure 12b), and their signs show opposite patterns. At lower level (0~30m), Cond is negative and Vmix is positive, which is the same as their ground characteristics. At upper level (30~200m), Cond is positive and Vmix is negative instead, indicating that cloud water is produced by vapor condensation at upper level and then being entrained to ground. The significant positive Cond supports that BLLJ-related moisture advection promotes vapor condensation and low stratus formation above surface, and the significant positive Vmix may indicate that the low stratus favours ground fog formation by turbulent exchange of LWC.

## 4. Discussions

Previous studies have elucidated the qualitative reasons for fog propagation. In this study, we describe the feature of fast fog propagation and identify its key impact factors more quantitatively. Figure 13 summarizes the mechanism of fog propagation. During the nighttime, a southerly BLLJ controls the study region, and the jet core intensity is about 10m/s which occurs at about 200m. The ground fog propagates northwestward with the speed of 9.6m/s. The BLLJ favours the fast fog propagation by three possible mechanisms: 1) BLLJ transports sufficient vapor from ocean to inland area. The turbulence strengthened by wind speed shear further moistens the PBL and promotes vapor condensation. This could be the dominant mechanism. 2) BLLJ transports warmer air from ocean to inland area and deepens the inversion layer. The strengthened inversion favours the accumulation of vapor and condensation nuclei. 3) The strong moisture advection could promote the low stratus formation in the downstream area, and later it subsides to be ground fog by turbulent exchange of cloud droplets. The stratus lowering phenomenon needs to be verified by additional observations.

The results could facilitate the understanding of cloud formation and development. Clouds, such as convective clouds, can develop and expand extraordinarily fast under strong synoptic forcing or unstable conditions. Fog can be viewed as a kind of near-surface stratus cloud, which usually forms under stable conditions with weak synoptic forcings. However, as revealed in this study, it can also develop and propagate fast under the effect of BLLJ. The quantitative relations between BLLJ and fog fast propagation may have implications on the cloud formation and development mechanism under stable synoptic conditions.

## 5. Conclusions

Previous studies have found that the spatial propagation of fog could be rather fast under favourable conditions, and the boundary layer low-level jet (BLLJ) could be a potential reason. In this study, we analyze the fast spatial propagation feature of a large-scale fog event in Jiangsu Province, China by high spatiotemporal resolution ground and satellite observations. The key impact factors and mechanisms of the BLLJ effect on fast spatial propagation are quantitatively revealed by WRF model simulations. Results show that:

The fog initials at 22:00 on 20 January 2020 over Jiangsu coastal area, and it reaches the west boundary of Jiangsu at 07:00 next day. Satellite retrievals show that the southeast side of fog area varies slightly but the northwest side expands fast, with the maximum propagation speed of 9.6m/s. During the fog period, the ground wind direction is consistent with fog propagation, which favours the vapor transportation from ocean and promotes fog formation. However, the wind speed (<3m/s) is at least one-third less than the fog propagation speed. Therefore, the ground meteorologies are insufficient to explain the fast propagation of fog. The influencing factors and mechanisms need to be investigated by exploring the PBL characteristics through numerical simulations.

The WRF model well simulates the temporal variation of meteorologies and reproduces the spatiotemporal evolution of fog area. A BLLJ (>6m/s) exists at the height between 50 and 500m. The jet core occurs at 1000hpa (200m) with the southeasterly winds of 10m/s, which can fit the propagation direction and speed of fog. Therefore, the southeasterly BLLJ is hypothesized to be the cause of fast propagation. BLLJ creates favourable PBL conditions by transporting moisture and warm air from ocean. The moisture advection and the vapor turbulent mixing generated by wind speed shear increase the humidity within PBL, and the propagation of fog area coincides with the movement of high humidity zone (vapor mixing ratio>4g/kg). The warm advection from ocean deepens inversion layer and additionally favours the accumulation of moisture and condensation nuclei. Additionally, it is found that low stratus could form above surface and subsides to be ground fog within 0~20min. The moisture advection is also responsible for the formation of low stratus.

Sensitive experiments quantitatively reveal the contributions of moisture advection and temperature advection to fog propagation. When moisture (temperature) advection is turned off, the fog area decreases by 62% (50%) and the propagation speed decrease by about 4.6m/s (5.2m/s). Process analysis on fog liquid water content (LWC) further illustrates the mechanism of fog propagation. Condensation (Cond) and LWC turbulent exchange (Vmix) are two important physical processes. At upper level (30~200m), Cond is positive and Vmix is negative. It indicates that BLLJ-related moisture advection significantly promotes condensation and probably favours low stratus formation. At ground and lower level (0~30m), Cond is basically negative and Vmix is positive. It indicates that cloud droplets at upper level are entrained downward by turbulent mixing, leading to the subsequent formation of ground fog. The stratus lowering phenomenon needs to be verified by additional observations.

In this study, by combination of observations and simulations, we have revealed the effect of southeasterly BLLJ on fog propagation, and quantified the contributions of BLLJ-related moisture advection and temperature advection to fog propagation. Three possible mechanisms are concluded: 1) Moisture advection from ocean promotes vapor condensation in downstream area, which could be the dominant cause; 2) Warm advection from ocean deepens inversion layer and additionally promote vapor accumulation within PBL. 3) The moisture advection probably promotes low stratus formation first, and later it subsides to be ground fog by turbulent mixing of cloud droplets. The coexistence of fast fog propagation and BLLJ is not a common phenomenon, so finding more cases requires additional work. It should be addressed in future studies in order to deeply understand the relationships between fog propagation and BLLJ under different regions and synoptic conditions. Their quantitative relationships could facilitate the understanding of cloud formation and development under stable synoptic conditions, since fog can be viewed as near-surface stratus cloud that can potentially propagate fast under stable conditions.

*Code and data availability*. Some of the data repositories have been listed in Section 2. The other data, model outputs and codes can be accessed by contacting Duanyang Liu via liuduanyang2001@126.com.

*Author contributions*. SY performed the model simulation, data analysis and manuscript writing. HW and DL proposed the idea, supervised this work and revised the manuscript. XL helped the revision of the manuscript. FZ provided and analyzed the observation data.

*Competing interests*. The authors declare that they have no conflict of interest.

*Acknowledgements*. This work is supported by the Special Project of Innovative Development of CMA (CXFZ2023J022), Open Research Foundation of Jiangsu Marine Meteorology (HYQX2022), Beijige Foundation (BJG202307), Research Foundation of Jiangsu Meteorology Bureau (KM202307), Basic Research Fund of CAMS (2022Y025).

# References

Andreas, E.L., Claffy, K.J., and Makshtas, A.P.: Low-level atmospheric jets and inversions over the western Weddell Sea, Boundary Layer Meteorol, 97(3), 459–486, https://doi.org/10.1023/A:1002793831076, 2000.

Bott, A.: On the influence of the physico-chemical properties of aerosols on the life cycle of radiation fogs, J. Aerosol Sci, 21(1-2), 1–31, https://doi.org/10.1007/BF00119960, 1991.

Boutle, I., Price, J., Kudzotsa, I., Kokkola, H., and Romakkaniemi, S.: Aerosol-fog interaction and the transition to well-mixed radiation fog, Atmos. Chem. Phys., 18(11), 1–19, https://doi.org/10.5194/acp-18-7827-2018, 2017.

Cermak, J. and Bendix, J.: A novel approach to fog/low stratus detection using Meteosat 8 data, Atmos. Res., 87(3-4), 279–292, https://doi.org/10.1016/j.atmosres.2007.11.009, 2008.

Dhangar, N. G., Lal, D. M., Ghude, S. D., Kulkarni, R., and Rajeevan, M.: On the conditions for onset and development of fog over new delhi: an observational study from the wifex, Pure Appl. Geophys, 673, 1-20, https://doi.org/10.1007/s00024-021-02800-4, 2021.

Dorman, C.E., Hoch, S.W., Gultepe, I., Wang, Q., Yamaguchi, R., Fernando, H., Krishnamurthy, R.: Large-Scale Synoptic Systems and Fog During the C-FOG Field Experiment. Boundary-Layer Meteorol, 181, 171–202, https://doi.org/10.1007/s10546-021-00641-1, 2021.

Dupont, J., Haeffelin, M., Protat, A., Bouniol, D., Boyouk, N., and Morille, Y.: Stratus–Fog Formation and Dissipation: A 6-Day Case Study, Boundary-Layer Meteorol, 143, 207–225, https://doi.org/10.1007/s10546-012-9699-4, 2012.

Di Vittorio, A. V. and Emery, W. J.: An automated, dynamic threshold cloud-masking algorithm for daytime AVHRR images over land, IEEE Trans. Geosci, 40, 1682–1694, https://doi.org/10.1109/TGRS.2002.802455, 2002.

Fathalli, M., Lac, C., Burneta, F., and Vié, B.: Fog due to stratus lowering: Experimental and modelling case study, Q. J. R. Meteorol, 148(746), 2299–2324. https://doi.org/10.1002/qj.4304, 2022.

Gao, S., Lin, H., Shen, B., and Fu, G.: A heavy sea fog event over the Yellow Sea in March 2005: Analysis and numerical modeling, Adv Atmos Sci, 24, 65-81, https://doi.org/10.1007/s00376-007-0065-2, 2007.

Gao, Y., Liu, D., Yan, S., Zhou, W., Wang, H., Zu, F., Mei, Q., Yi, C., and Sheng, Y.: Influence of sea-land breeze on formation and dissipation of severe dense fog and its explosive enhancement in the Yellow Sea Coastal Area, Sci. China Earth Sci., 2023. (accepted; under translation into English)

Gultepe, I., Tardif, R., Michaelides, S. C., Cermak, J., Bott, A., Bendix, J., Muller, M. D., et al.: Fog research: a review of past achievements and future perspectives, Pure Appl. Geophys, 164, 1121–1159, https://doi.org/10.1007/s00024-007-0211-x, 2007.

Haeffelin, M., Bergot, T., Elias, T., Tardif, R., Carrer, D., Chazette, P., and Zhang, X.: PARISFOG: Shedding new light on fog physical processes, Bull Am Meteorol Soc, 91(6), 767-783, https://doi.org/10.1175/2009bams2671.1, 2010.

Jia, X., Quan, J., Zheng, Z., Liu, X., Liu, Q., He, H., and Liu, Y.: Impacts of anthropogenic aerosols on fog in North China Plain, J. Geophys. Res.-Atmos., 124, 252–265, https://doi.org/10.1029/2018jd029437, 2018.

Jiao, S., Zhu, C., Zhu, Y., Yuan, C., Zu, F., and Sun, K.: A discussion on the reason for a rare persistent heavy fog event in Jiangsu Province, Acta Meteorol. Sin, 74, 200–212, https://doi.org/10.11676/qxxb2016.015, 2016.

Koračin, D., Dorman, C. E., Lewis, J. M., Hudson, J. G., Wilcox, E. M., and Torregrosa, A.: Marine fog: A review, Atmos. Res., 143, 142-175, https://doi.org/10.1016/j.atmosres.2013.12.012, 2014.

Korb, G. and Zdunkowski, W.: Distribution of radiative energy in ground fog, Tellus, 22(3), 298-320, https://doi.org/10.3402/tellusa.v22i3.10223, 1970.

Kraus, H., Malcher, J., and Schaller, E.: A nocturnal low level jet during PUKK, Boundary Layer Meteorol, 31, 187-195, https://doi.org/10.1007/BF00121177, 1985.

Kunkel, B. A.: Parameterization of Droplet Terminal Velocity and Extinction Coefficient in Fog Models, J. Appl. Meteorol, 23(1), 34–41, https://doi.org/10.1175/1520-0450(1984)023<0034:PODTVA>2.0.CO;2, 1983.

Li, P. and Fu, G.: The Formation Mechanism of a Spring Sea Fog Event over the Yellow Sea Associated with a Low-Level Jet, Weather and Forecasting, 27(6), 1538-1553, https://doi.org/10.1175/WAF-D-11-00152.1, 2012.

Li, Z. H., Liu, D. Y., Yang, J.: The microphysical processes and macroscopic conditions of the radiation fog droplet spectrum broadening, Chinese J. Atmospheric Sci., 35, 41–54, https://doi.org/10.3878/j.issn.1006-9895.2011.01.04, 2011. (in Chinese)

Li, Z., Liu, D., Yan, W., Wang, H., Zhu, C., Zhu, Y., and Zu, F.: Dense fog burst reinforcement over Eastern China: A review, Atmos. Res., 230(D19), 104639, https://doi.org/10.1016/j.atmosres.2019.104639, 2019.

Liu, D., Yang, J., Niu, S., and Li, Z.: On the Evolution and Structure of a Radiation Fog Event in Nanjing, Adv Atmos Sci, 28(1), 223-237, https://doi.org/10.1007/s00376-010-0017-0, 2011.

Liu, D. Y., Niu, S. J., Yang, J., Zhao L., Lv, J., and Lu, C.: Summary of a 4-year fog field study in Northern Nanjing, part 1: fog boundary layer, Pure Appl. Geophys, 169, 809–819, https://doi.org/10.1007/s00024-011-0343-x, 2012.

Liu, D., Yan, W., Yang, J., Pu, M., Niu, S., Li, Z.: A Study of the Physical Processes of an Advection Fog Boundary Layer, Boundary Layer Meteorol, 158(1), 125-138, https://doi.org/10.1007/s10546-015-0076-y, 2016.

Liu, D., Li, Z., Yan, W., and Li, Y.:. Advances in fog microphysics research in China, Asia Pac J Atmos Sci, 53(1), 131–148, https://doi.org/10.1007/s13143-016-0028-6, 2017.

Liu, Q., Wang, Z. Y., Wu, B. G., Liu, J. L., and Gultepe, I.: Microphysics of fog bursting in polluted urban air, Atmospheric Environ., 10, 118357, https://doi.org/10.1016/j.atmosenv.2021.118357, 2021.

Nakanishi, M.: Large-eddy simulation of radiation fog. Boundary Layer Meteorol, 94, 461-493, https://doi.org/10.1023/A:1002490423389, 2000.

Pleim, J. E., Gilliam, R.: An indirect data assimilation scheme for deep soil temperature in the Pleim-Xiu land surface model, J. Appl. Meteorol, 48, 1362-1376, https://doi.org/10.1175/2009JAMC2053.1, 2009.

Pu, M. J., Zhang, G. Z., Yan, W. L., and Li, Z. H.: Features of a rare advection-radiation fog event, Sci. China Earth Sci., 51(7), 1044–1052, https://doi.org/10.1007/s11430-008-0071-y, 2008.

Quan, J., Liu, Y., Jia, X., Liu, L., Dou, Y., Xin, J., and Seinfeld, J. H.: Anthropogenic aerosols prolong fog lifetime in China, Environ. Res. Lett., 16(4), 044048, https://doi.org/10.1088/1748-9326/abef32, 2021.

Schwenkel, J. and Maronga, B.: Large-eddy simulation of radiation fog with comprehensive two-moment bulk microphysics: impact of different aerosol activation and condensation parameterizations, Atmos. Chem. Phys., 19(10), 1-23, https://doi.org/10.5194/acp-19-7165-2019, 2018.

Shao, N., Lu, C., Jia, X., Wang, Y., Li, Y., Yin, Y., Zhu, B., Zhao, T., Liu, D., Niu, S., Fan, S., Yan, S., and Lv, J.: Radiation fog properties in two consecutive events under polluted and clean conditions in the Yangtze River Delta, China: a simulation study, Atmos. Chem. Phys., 23, 9873–9890, https://doi.org/10.5194/acp-23-9873-2023, 2023.

Shen, P., Liu, D., Gultep, I., Lin, H., Cai, N., and Cao, S.: Boundary layer features of one winter fog in the Yangtze River Delta, China, Pure Appl. Geophys, 179(9), 3463-3480, https://doi.org/10.1007/s00024-022-03119-4, 2022.

Steeneveld, G. J., Ronda, R. J., and Holtslag, A. A. M.: The Challenge of Forecasting the Onset and Development of Radiation Fog Using Mesoscale Atmospheric Models, Boundary Layer Meteorol, 154(2), 265–289, https://doi.org/10.1007/s10546-014-9973-8, 2014.

Sukoriansky, S., Galperin, B., Perov, V.: Application of a new spectral model of stratified turbulence to the atmospheric boundary layer over sea ice, Boundary Layer Meteorol, 117, 231–257, https://doi.org/10.1007/s10546-004-6848-4, 2005.

Tian, M., Wu, B., Huang, H., Zhang, H., Zhang, W., and Wang, Z.: Impact of water vapor transfer on a Circum-Bohai-Sea heavy fog Observation and numerical simulation, Atmos. Res., 229, 1-22, https://doi.org/10.1016/j.atmosres.2019.06.008, 2019.

van der Velde, I. R., Steeneveld, G. J., Wichers Schreur, B. G. J., and Holtslag, A. A. M.: Modeling and Forecasting the Onset and Duration of Severe Radiation Fog under Frost Conditions, Mon Weather Rev, 138(11), 4237–4253, https://doi.org/10.1175/2010mwr3427.1, 2010.

Wang, H., Zhang, Z., Liu, D., Zhu, Y., Zhang, X., and Yuan, C.: Study on a Large-Scale Persistent Strong Dense Fog Event in Central and Eastern China, Adv. Meteorol, 4, 1–15, https://doi.org/10.1155/2020/8872334, 2020.

Wang, Y., Lu, C., Niu, S., Lv, J., Jia, X., Xu, X., et al.: Diverse dispersion effects and parameterization of relative dispersion in urban fog in eastern China, J. Geophys. Res.-Atmos., 128, e2022JD037514, https://doi.org/10.1029/2022JD037514, 2023.

Wei, W., Zhang, H. S., Ye, X. X.: Comparison of low-level jets along the north coast of China in summer, J. Geophys. Res.-Atmos., 119(16), 9692–9706, https://doi.org/10.1002/2014JD021476, 2014.

Wobrock, W., Schell, D., Maser, R., Kessel, M., Jaeschke, W., Fuzzi, S., and Bendix, J.: Meteorological characteristics of the Po Valley fog, Tellus B, 44(5), 469-488, https://doi.org/10.3402/tellusb.v44i5.15562, 1992.

Wu, B., Li, Z., Ju, T., and Zhang, H.: Characteristics of Low-level jets during 2015–2016 and the effect on fog in Tianjin, Atmos. Res., 245, 105102, https://doi.org/10.1016/j.atmosres.2020.105102, 2020.

Yan, S., Zhu, B., Zhu, T., Shi, C., Liu, D., Kang, H., Lu, W., and Lu, C.: The effect of aerosols on fog lifetime: observational ev-idence and model simulations, Geophys. Res. Lett, 48(2), e2020GL61803, https://doi.org/ 10.1029/2020GL091156, 2021.

Yang, Y., Hu, X.-M., Gao, S., and Wang, Y.: Sensitivity of WRF simulations with the YSU PBL scheme to the lowest model level height for a sea fog event over the Yellow Sea, Atmos. Res., 215, 253–267, https://doi.org/10.1016/j.atmosres.2018.09.004, 2019.

Ye, X., Wu, B., and Zhang, H.: The turbulent structure and transport in fog layers observed over the Tianjin area, Atmos. Res., 153, 217-234, https://doi.org/10.1016/j.atmosres.2014.08.003, 2015.

Zhang, G., Bian, L., Wang, J., Yang, Y., Yao, W., and Xu, X.: The boundary layer characteristics in the heavy fog formation pro-cess over beijing and its adjacent areas, Sci. China Earth Sci., 48, 88-101, https://doi.org/10.1360/05yd0029, 2005.

Zhou, B. and Ferrier, B.: Asymptotic Analysis of Equilibrium in Radiation Fog, J. Appl. Meteorol, and Climatology, 47, 1704-1722, https://doi.org/10.1175/2007JAMC1685.1, 2008.

Zhou, B. and Du, J.: Fog prediction from a multimodel mesoscale ensemble prediction system, Weather and Forecasting, 25(1), 303-322, https://doi.org/10.1175/2009WAF2222289.1, 2010.

Zhou, B., Du, J., Gultepe, I., and Dimego, G.: Forecast of low visibility and fog from NCEP: Current status and efforts, Pure Appl. Geophys., 169, 895-909, https://doi.org/10.1007/s00024-011-0327-x, 2012.

Zhu, Y., Zhu, C., Zu, F., Wang, H., Liu Q., Qi, M., and Wang, Y..: A persistent fog event involving heavy pollutants in Yancheng area of Jiangsu Province, Adv. Meteorol, 2018, 2512138, https://doi.org/10.1155/2018/2512138, 2018.

Zhu, Y., Li, Z., Zu, F., Wang, H., Liu, Q., Qi, M., and Wang, Y.: The propagation of fog and its related pollutants in the Central and Eastern China in winter, Atmos. Res., 265, 105914, https://doi.org/10.1016/j.atmosres.2021.105914, 2022.

Table 1. Model parameterization schemes and sensitive experiments

| Physical scheme | Option |
|---|---|
| Boundary layer | QNSE |
| Microphysics | Lin double moment |
| Longwave radiation | RRTM |
| Shortwave radiation | Goddard |
| Land surface | Pleim-Xiu |
| Cumulus | Grell-3D |
| Grid nudging | Off |
| Observation nudging | Off |
| **Experiment** | **Description** |
| Base | The base condition |
| Tadv0 | Turning off temperature advection |
| QvAdv0 | Turning off water vapor advection |
| QcAdv0 | Turning off cloud water advection |
| NoAdv | Turning off all advections above |

Table 2. The times when visibility reaches 1000m, 500m and 200m at three representative stations. (DF:Dafeng, BY:Baoying, SH:Sihong).

| | | Formation (Vis=1000m) | | Vis=500m | | Vis=200m | |
|---|---|---|---|---|---|---|---|
| Station | Location | Time | Wind | Time | Wind | Time | Wind |
| DF | 120.48°E,33.20°N | 19:45 | 1.3m/s, E | 22:55 | 1.2m/s, E | 23:45 | 1.3m/s, E |
| BY | 119.30°E,33.23°N | 01:25 | 1.2m/s, ESE | 03:15 | 1.4m/s, ESE | 03:45 | 1.3m/s, SE |
| SH | 118.22°E,33.48°N | 04:50 | 1.6m/s, ESE | 06:10 | 1.3m/s, ESE | 07:15 | 2.4m/s, ESE |
| | Distance (km) | Time difference (h) | | Time difference (h) | | Time difference (h) | |
| DF-BY | 110 | 4.7 | | 4.3 | | 4.0 | |
| BY-SH | 105 | 3.4 | | 2.9 | | 3.5 | |

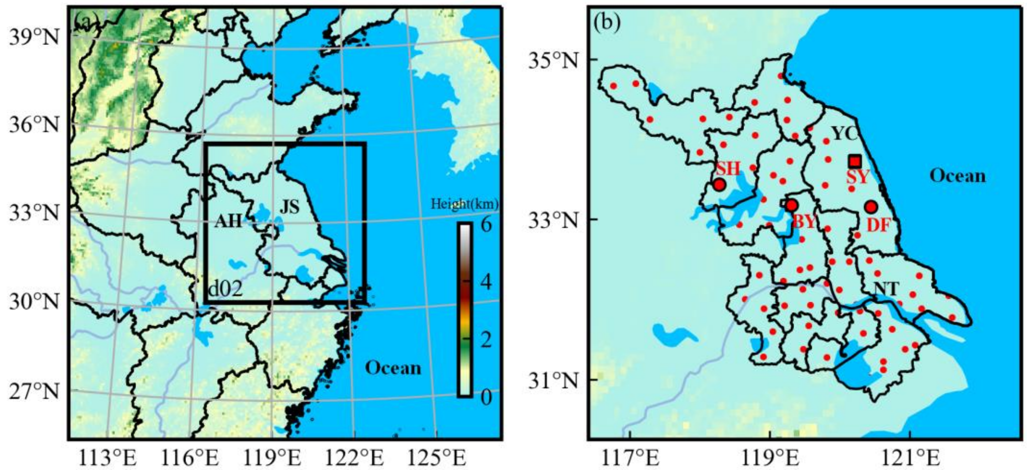


Figure 1. The parent and nest model domain. The shaded color is terrain height. The red points are automatic weather stations in Jiangsu, China. The three larger circle points are Sihong (SH), Baoying (BY), and Dafeng (DF) stations, and the square point is Sheyang (SY) sounding station. The black labels are some province or city names. (JS:Jiangsu Province; AH:Anhui Province; YC:Yanchen; NT:Nantong).

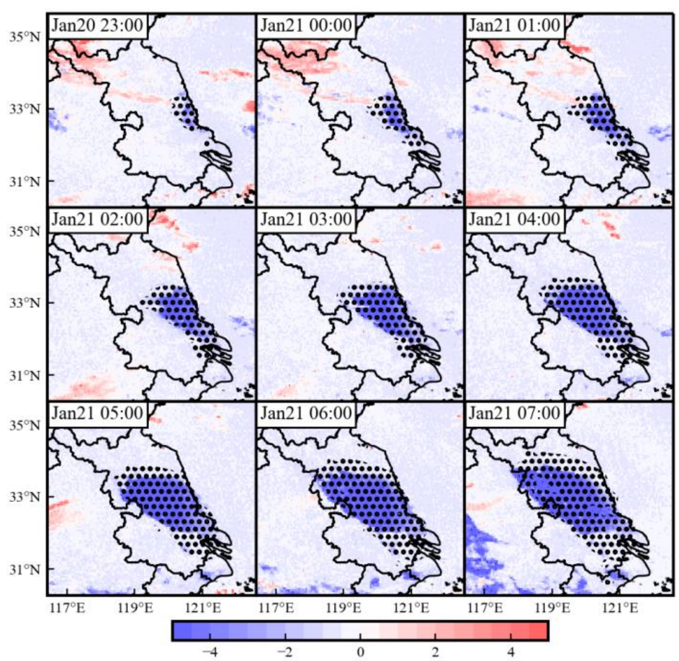


Figure 2. The spatial evolution of fog. The black dots are simulated fog areas. The shaded colors are satellite observed brightness temperature difference (3.9μm minus 11.2μm), where the blue colors (smaller than -2 K) indicate the fog areas.

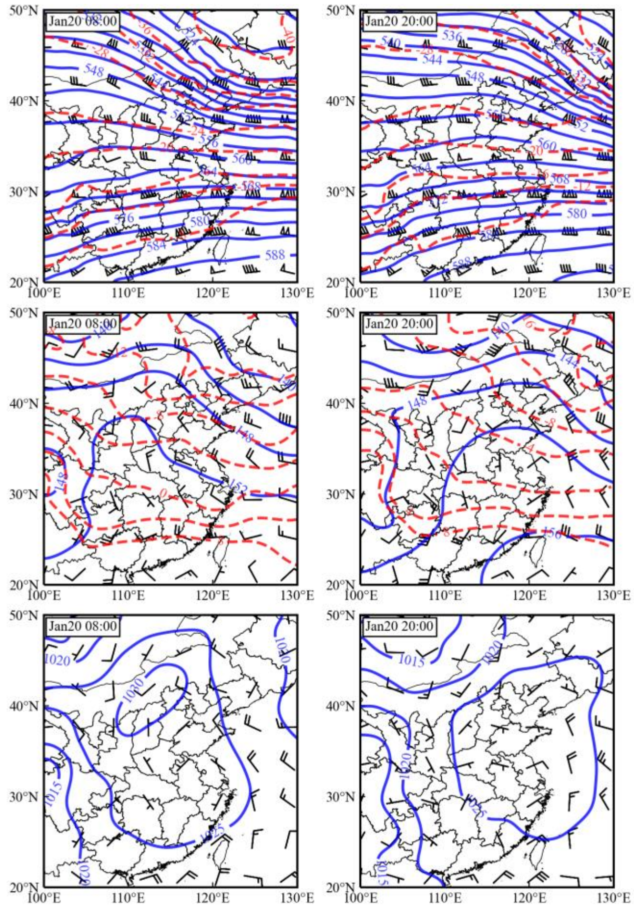


Figure 3. The synoptic background of 500hpa (first row), 850hpa (second row) and surface (third row) at 08:00 and 20:00 on 20 January 2020.

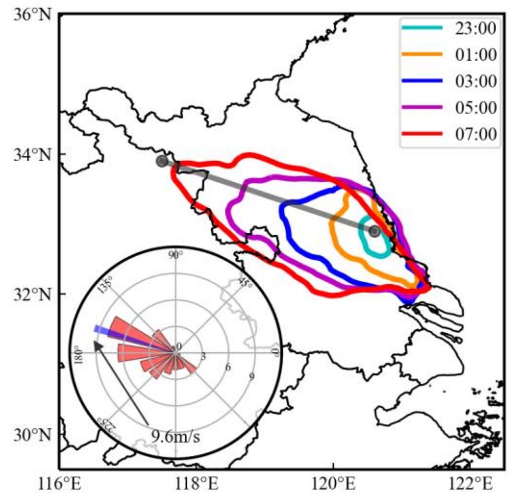


Figure 4. The colored curves are the fog boundaries (satellite retrievals) from 23:00 on 20 January to 07:00 next day every 2 hours. Fog boundaries from small to large represent 23:00, 01:00, 03:00, 05:00 and 07:00, respectively. The gray straight line indicates the fog propagation direction, and the vertical features of meteorologies at this line will be analyzed in Figures 7, 8, and 9. The lower-left polar plot is the fog propagation speed at 16 directions (22.5° interval), and the narrow blue bar highlights the maximum propagation speed (9.6m/s) occurring at 160° direction (in Cartesian coordinate system) (from southeast to northwest).

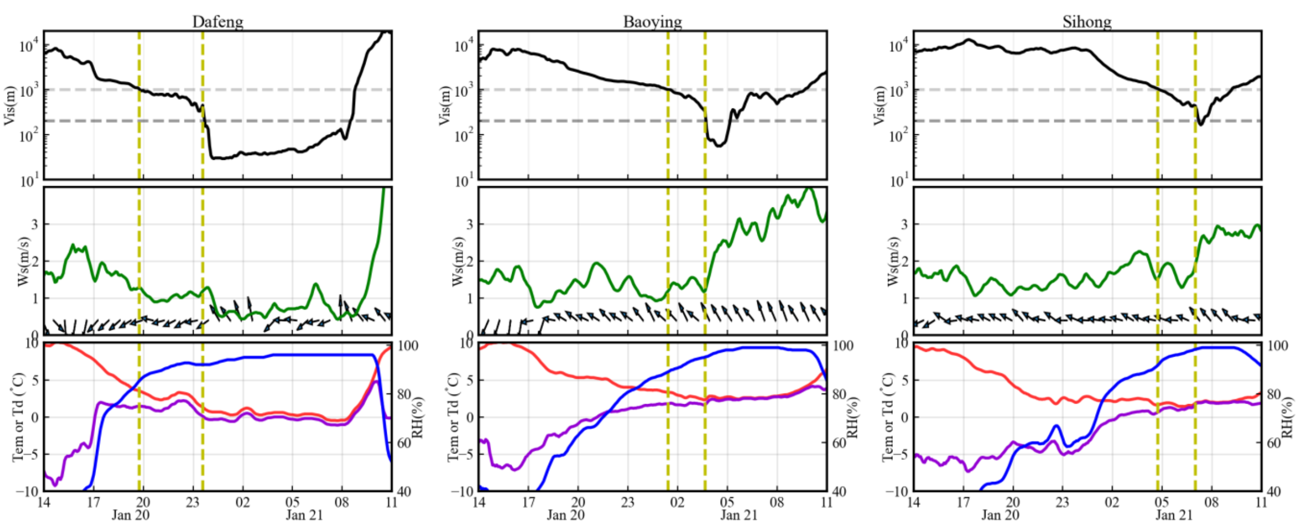


Figure 5. The temporal variation of ground visibility (Vis; black line), wind speed (Ws; green line), wind direction (vectors), temperature (Tem; red line), dew point (Td; violet line) and relative humidity (RH; blue line) at Dafeng, Baoying, and Sihong stations. The horizontal dashed lines are visibilities of 1000m and 200m. The vertical dashed lines mark the times of fog formation and visibility burst dropping.

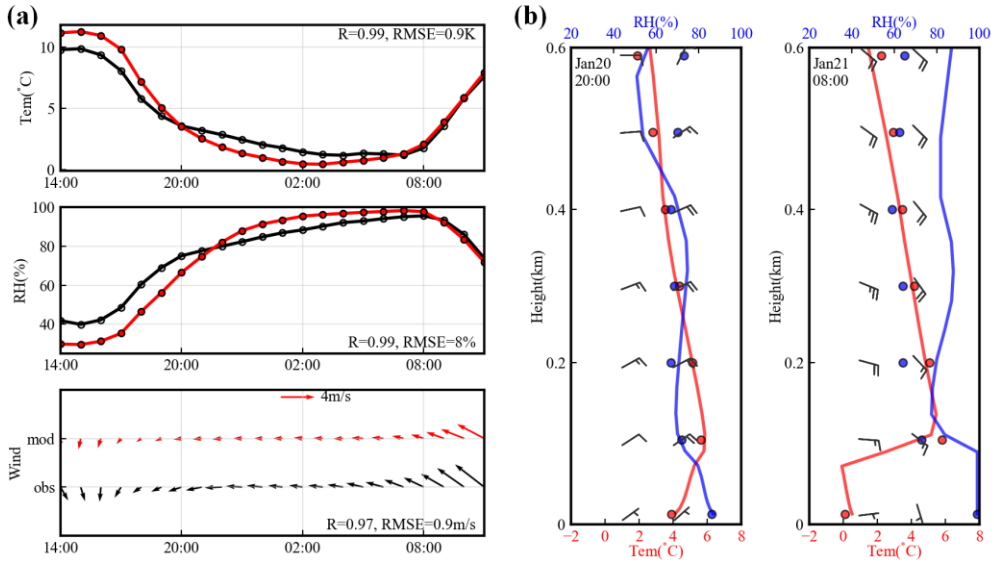


Figure 6. (a) The model performance on 2m Temperature (Tem), 2m Relative humidity (RH) and 10m wind speed and direction. The red color is simulation and black color is observation. The time is from 14:00 on 20 January 2020 to 11:00 next day. (b) The model performance on temperature (red), RH (blue) and wind (barbs) profiles at Sheyang sounding station. For temperature and RH, the observations are scatters and simulations are solid lines. For wind barbs, the left column is observations and the right column is simulations. The scatters and barbs are interpolated onto 0~600m every 100m.

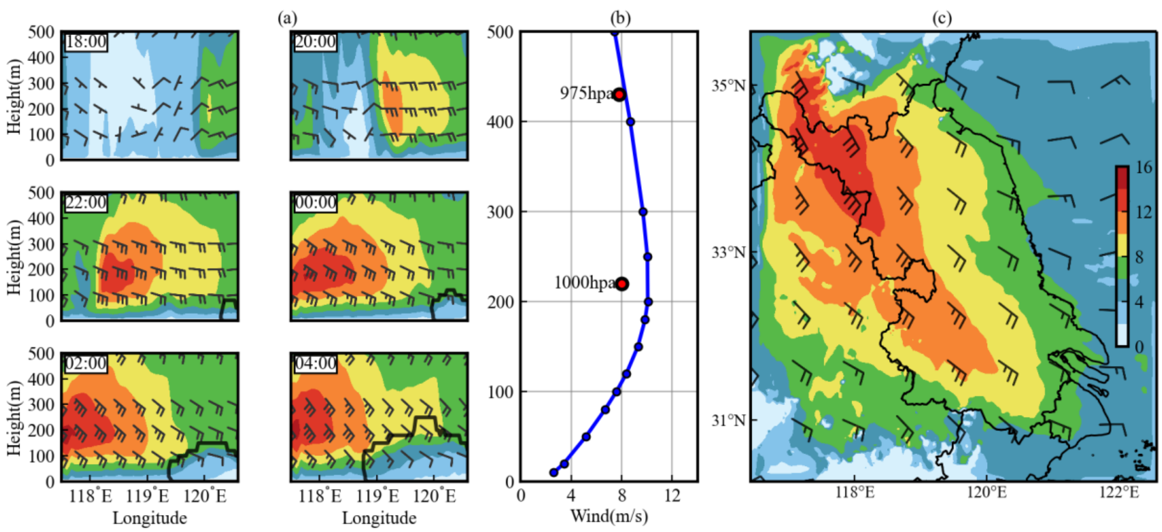


Figure 7. (a) The height-longitude variation of horizontal wind direction (vectors) and wind speed (shaded colors) at the crossing line in Figure 4. The lower-right black polygons are the fog area. The times are from 18:00 on 20 January to 04:00 next day. (b) The averaged wind speed profile at the crossing line during 23:00~07:00. The two red points are the wind speed calculated from ERA5 reanalysis. (c) The averaged wind direction (vectors) and wind speed (shaded colors) at 1000hpa during 23:00~07:00.

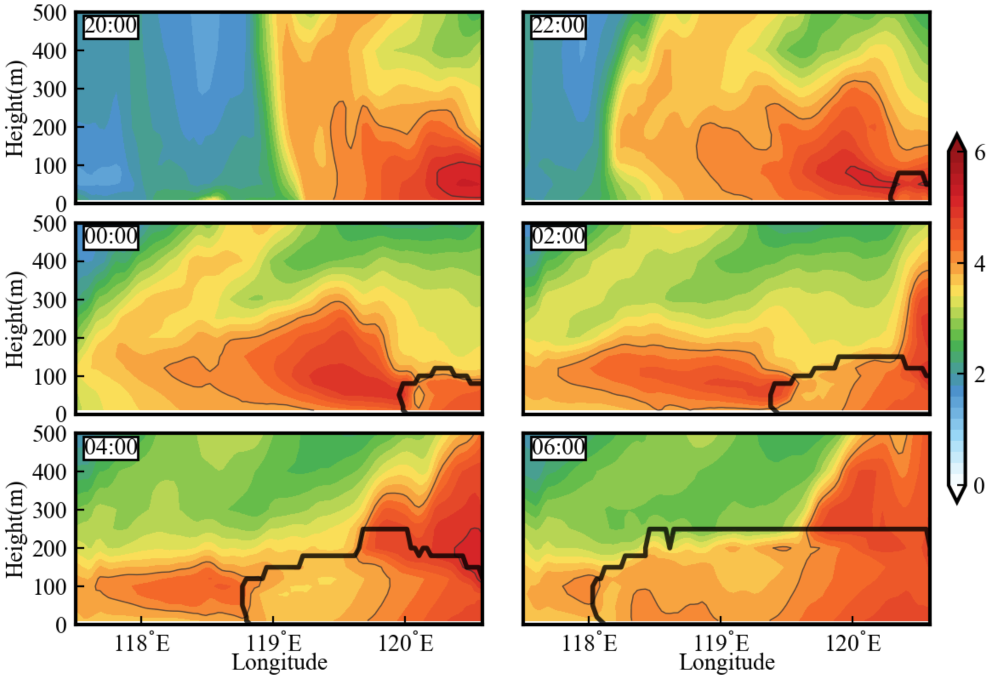


Figure 8. The height-longitude distribution of water vapor mixing ratio (g/kg) at the crossing line in Figure 4. The deep black polygons are the fog area. The light black lines are the region of water vapor mixing ratio larger than 4g/kg. The times are from 20:00 on 20 January to 06:00 next day.

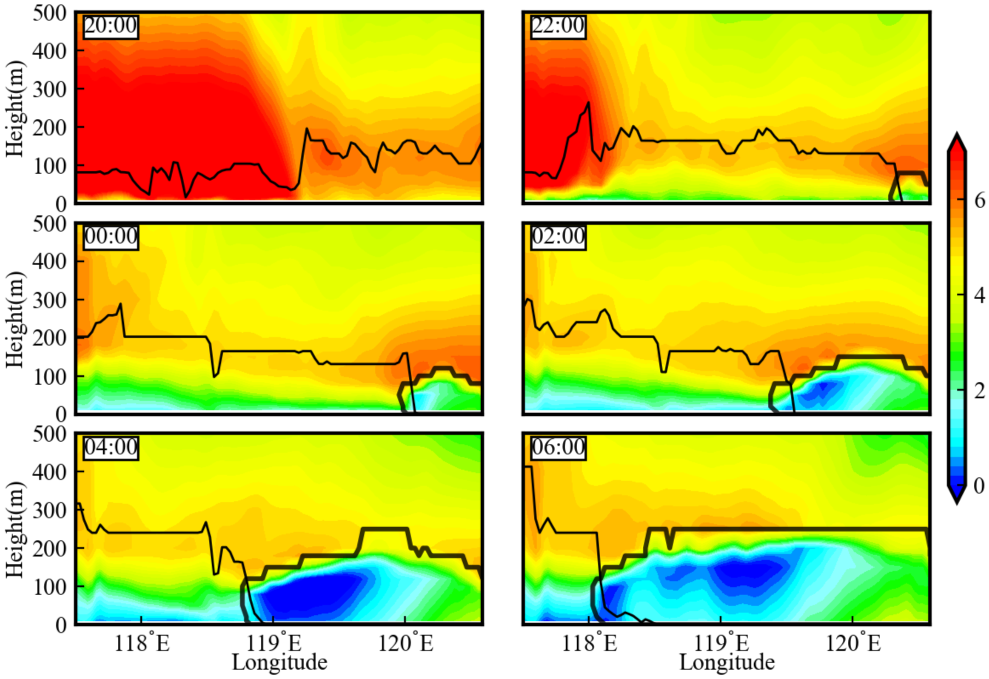


Figure 9. Same as the previous figure, but for the temperature. The bold black polygons are the fog area. The thin black lines are the top of inversion layer.

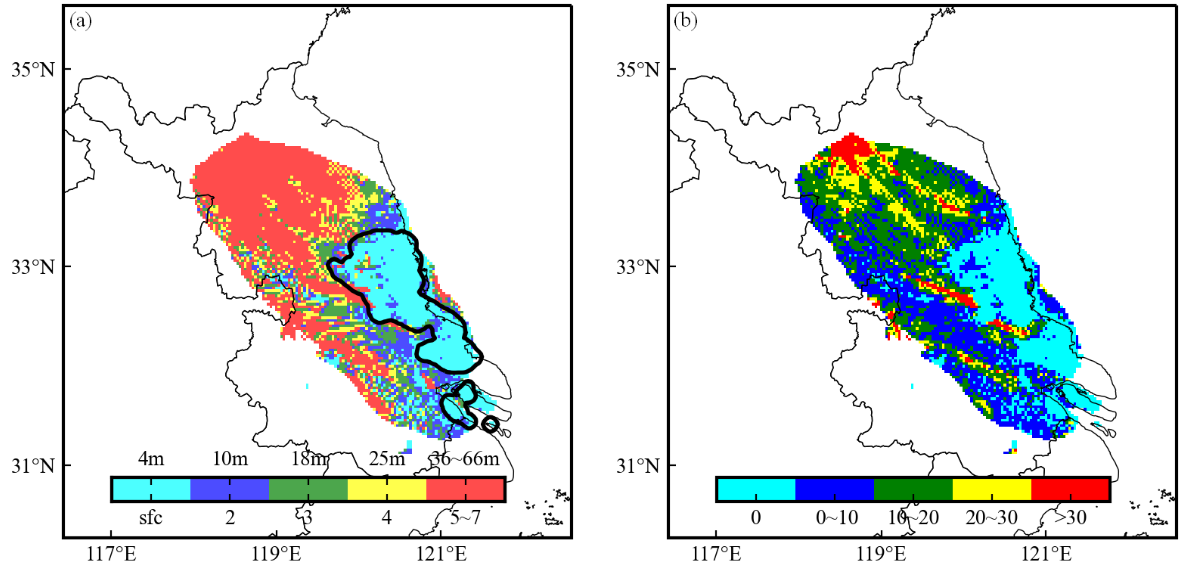


Figure 10. (a) The height (shaded color) at which fog/low stratus firstly forms. The black contours are the ground fog areas at 00:00 on 21 January 2020. The colorbar represents the model level and the corresponding height above surface. For example, the cyan colors indicate that fog firstly forms at the surface level with the corresponding height of about 4m. The red colors indicate that low stratus firstly forms at the $5^{th}$ to $7^{th}$ model level with the corresponding height of about 36~66m. (b) The time differences between ground fog formation and low stratus formation. For example, the cyan colors indicate that fog firstly forms at ground. The blue colors indicate that the ground fog forms 0~10min later than the low stratus formation.

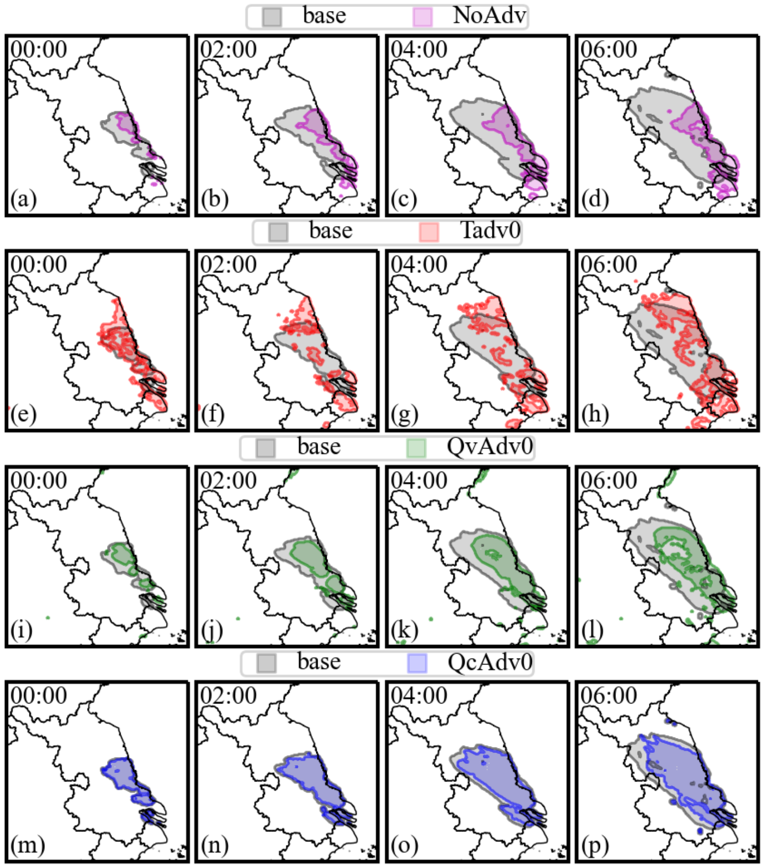


Figure 11. The temporal variation of ground fog area under different experiments from 00:00 to 06:00 on 21 January. The black color is the base experiment. The Tadv0 (red), QvAdv0 (green) and QcAdv0 (blue) are the experiments turning off temperature advection, moisture advection and cloud water advection, respectively. The NoAdv (pink) is the experiment turning off all of the above advections.

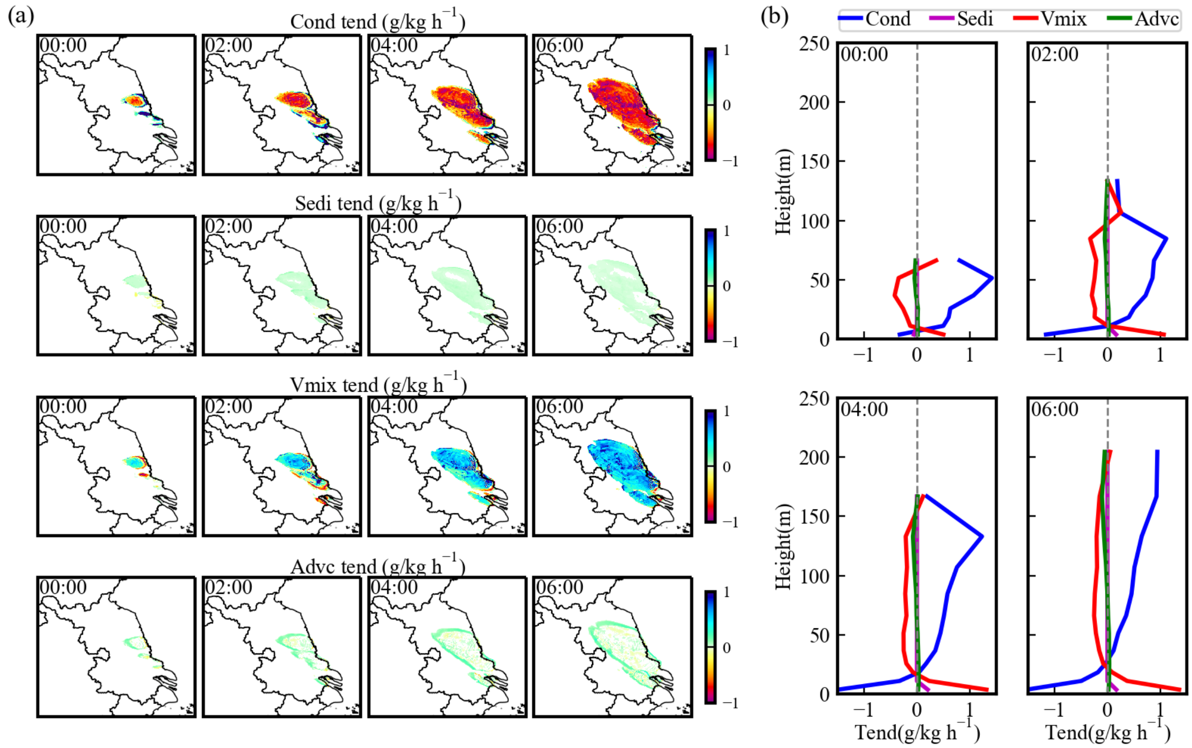


Figure 12. (a) The spatial distribution of the four process tendencies contributing to LWC variation at ground level. (b) The vertical profiles of the process tendencies averaged in fog area. The times are from 00:00 to 06:00 on 21 January. (Cond:condensation or evaporation; Sedi:sedimentation; Vmix:turbulent exchange; Advc:horizontal and vertical advection).

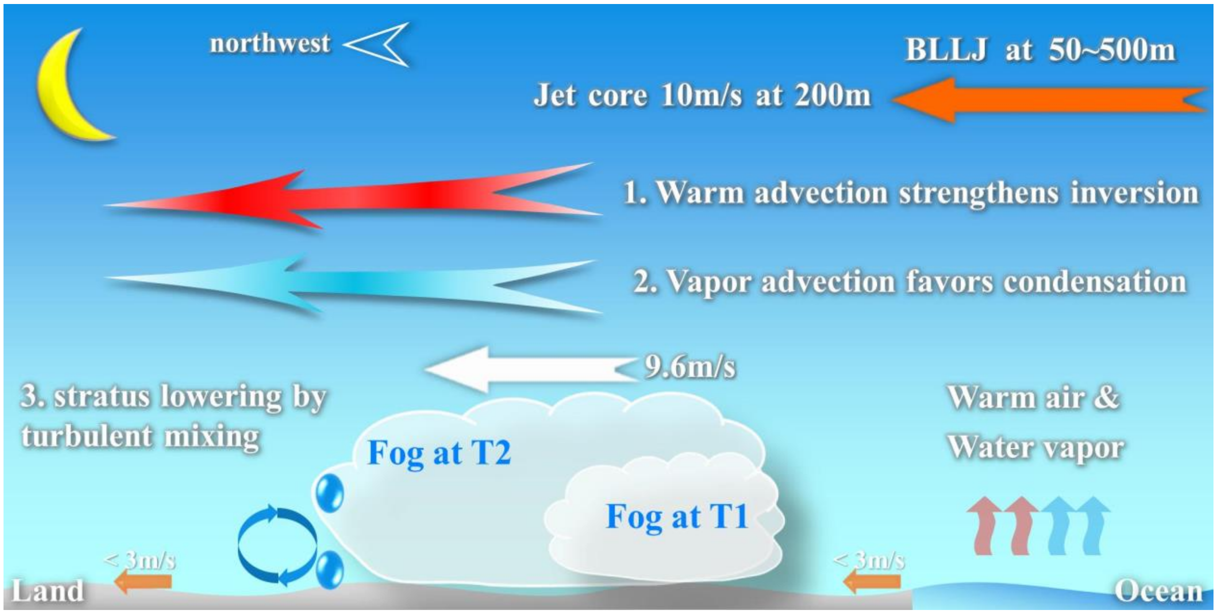


Figure 13. The concept diagram of fog propagation. The ground wind speed (short orange arrows) is generally less than 3m/s. A southeasterly BLLJ exists at the height from 50 to 500m, and the jet core intensity is 10m/s at 200m (the long orange arrow). The updraft arrows represent the warm and wet air from ocean. The two cloud shapes are fog areas at two adjacent times, and the white arrow indicates the fog propagation speed (9.6m/s). The fog propagation is probably caused by three approaches: 1) Moisture advection from ocean promotes vapor condensation in the downstream area, which could be the dominant cause (the blue fancy arrow); 2) Warm advection from ocean deepens inversion layer and additionally promotes vapor accumulation within PBL (the red fancy arrow); 3) The moisture advection probably result in the low stratus formation, and later it subsides to ground by turbulent mixing of cloud droplets (the blue water drops and circular arrows). Note that warm and moisture advections occur at nearly all heights below 500m, not merely at the height indicated by arrows.